EFFECT OF CURING TEMPERATURE ON CEMENT HYDRATION

IMAD ELKHADIRI, MARTA PALACIOS, FRANCISCA PUERTAS

Eduardo Torroja Institute for Construction Sciences (CSIC)
Serrano Galvache, 4, 28033 Madrid, Spain

E-mail: puertasf@ietcc.csic.es

Submitted July 16, 2008; accepted February 6, 2009

Keywords: Calcium-silica-hydrate (C–S–H), Compressive strength, Curing temperature, Microstructure

Hydration was studied in two cements (CEM I 42.5R and CEM II/A-V 42.5R) cured at temperatures ranging from 4 to 85°C. Hydration was monitored with a number of instrumental techniques: X-Ray Diffraction (XRD), Fourier Transform Infrared Spectroscopy (FTIR), Backscattered Electron (BSE) imaging in conjunction with Energy Dispersive X-ray analysis (EDX) and Nuclear Magnetic Resonance (MAS NMR). The mechanical strength of the pastes was likewise determined at different [illegible] *term compressive strength. The decline in 28-day compressive strength in pastes cured at high temperatures was attributed* [illegible] *more intense in the calcium silica hydrate gel (C–S–H) formed in pastes cured at high temperatures than in the gel formed in pastes cured at low temperatures. No substantial temperature-induced differences were found between cements with and* [illegible]

INTRODUCTION

Portland cement hydration is affected by many variables, including chemical composition, the water/cement ratio, the presence of mineral additions and fineness. Yet another variable, however, is regarded to play a key role, bearing on early hydration kinetics and the properties of the hardened cement paste: that variable is temperature [1].

A recent paper [2] concluded that high curing temperatures raised the very early compressive strength of sulphate-resistant cement, but had an adverse effect on mechanical properties at curing times of over 15 days. On the contrary, in cement pastes cured at temperatures of 22°C or lower, mechanical strength was observed to develop throughout the curing process. The reason for these observations is that a high initial rate of hydration induces the non-uniform distribution of the hydration product across the microstructure, with dense clusters forming around the hydrating grains and retarding subsequent hydration. The resulting increase in porosity has an adverse effect on long-term strength [3, 4]. A study of early age porosity [2] showed that at 85°C total 28-day porosity increased by more than 20 % due to rising meso- and macro-porosity, which would explain the decline in strength in pastes cured at 85°C. Such greater porosity also makes cement pastes more vulnerable to chemical attack by aggressive agents, reducing the service life of structures [5-8]. Parry-Jones et al. [9-11] studied hydration in cement pastes cured for up to 31 days at temperatures ranging from 20 to 80°C. These authors calculated the degree of hydration with ^{29}Si MAS NMR. For pastes hydrated at from 20 to 55°C, strength and degree of hydration were linearly correlated, but for a given degree of hydration the pastes hydrated at 80°C had perceptibly lower strength than the pastes cured at lower temperatures.

Curing temperature has a visible effect on C–S–H gel structure. A number of authors have reported rises in the degree of C–S–H gel polymerization with increasing hydration temperature [12, 13]. The degree of polymerization can be inferred from the $\sum Q^2/Q^1$ ratio using ^{29}Si MAS NMR spectra. According to Al-Dulaijan et al. [9], for a given degree of hydration, the $\sum Q^2/Q^1$ ratio, and consequently the rate of polymerisation, rose with temperature. Hirljac et al. [13] found that the main species identified in older age hydrated pastes cured at a high temperature were dimer, pentamer and octamer silica units. Elkhadiri and Puertas [2] found that increasing the curing temperature from 20 to 85°C raised the average C–S–H gel chain length dramatically, from two to eight links, even after only two days.

Curing temperature affects both the inner and outer C–S–H gel structure. Regourd and Gautier [14] reported that the outer C–S–H formed at 80°C was much more fibrous, exhibiting morphology reminiscent of pastes hydrated with calcium chloride accelerators.

Backscattered electron (BSE) imaging [5, 6, 8, 15, 16] showed that high temperature curing led to the formation of brighter rims around the cement grains regarded to constitute the inner C–S–H gel structure. Kjellsen et al. [5, 6] and Patel et al. [8] reported that

pastes hydrated at high temperatures exhibited brighter and thicker inner C–S–H rims than pastes hydrated at low temperatures. Such brightness is associated with several developments: an increase in the average atomic number, a decrease in the water content or both, or high sulphate concentration in C–S–H gels formed at high temperatures [17, 18].

Temperature affects the interaction between additions and cement compounds [19, 20, 21]. Alite hydration was found to rise sharply from a very early age in the presence of slag and volcanic ash, but much less abruptly when fly ash was the addition. Belite hydration was delayed in the presence of fly ash at 40 and 60°C, but was somewhat enhanced at lower temperatures.

Escalante et al. [20] noted that for all blended cement pastes an increase in curing temperature led to greater porosity, with the most prominent differences appearing between 10 and 60°C. The same authors confirmed that in fly ash-based pozzolanic cement pastes, $Ca(OH)_2$ was almost absent in pastes cured at 60°C, whereas at 10°C, clusters of $Ca(OH)_2$ were visible in the microstructure.

The present paper reports the results of a systematic study of hydration in two different cements, a fly ash-OPC blended cement, CEM II/A-V 42.5R (EN-197-1) and an ordinary Portland cement, CEM I 42.5R, at temperatures ranging between 4 and 85°C.

EXPERIMENTAL

The chemical composition of the two Spanish cements (CEM I 42.5R and CEM II/A-V 42.5R) used in this study is given in Table 1. Some physical and mechanical properties of these cements are shown in Table 2.

The cements were mixed with distilled water at a water/solid ratio of 0.3, cast in 1×1×6 cm^3 moulds and consolidated on a vibrating table. The specimens were cured in a humidity chamber (22 ± 2°C, 99% relative humidity), removed from the moulds after 24 h and then cured at temperatures of from 4 to 85°C for 2, 7, 15 or 28 days. Compressive strength tests were conducted at each age on specimens cured at each temperature.

After failure, the fragments obtained from the 2- and 28-day prisms were crushed and immersed in acetone and ethanol to interrupt hydration. These samples were subsequently placed in a vacuum dessicator.

The X-ray diffraction patterns for the powdered samples were recorded on a Philips PW-1710 diffractometer with a wavelength setting of 1.5406 ($\lambda Cu_{K\alpha}$).

Porosity was determined by mercury intrusion porosimetry using a Micromeritics 9320 porosimeter. The range defined to determine total porosity and pore size distribution was 200 to 0.068 μm.

An ATIMATTSON Genesis Fourier transform infrared (FTIR) spectrometer was used to determine the absorption bands for the hydrated compounds at a scan wavenumber 4000-400 cm^{-1}.

Morphological and micro-analytical data were collected on carbon-coated samples with a JEOL 5400 scanning electron microscope (SEM) coupled to an Oxford-Link SYSTEM ISIS backscattered detector (BSE/EDX) on carbon-coated samples.

The positions occupied by the ^{29}Si atoms were found with solid nuclear magnetic resonance (MAS NMR) techniques, using a Bruker MSL 400 spectrometer. The reference pattern used for the ^{29}Si spectra was tetramethyl-silane (TMS).

Table 1. Chemical composition of used cements (wt.%).

	CEM I 42.5R	CEM II/A-V 42.5R
SiO_2	18.86	22.55
Al_2O_3	5.50	8.06
Fe_2O_3	3.29	6.29
CaO	62.52	57.03
MgO	2.17	2.29
SO_3	3.33	3.37
Na_2O	0.15	0.15
K_2O	0.90	0.98
Loss of Ignition	3.28	2.02
CaO_{free}	1.34	1.51

Table 2. Physical and mechanical properties of used cements.

	CEM I42.5R	CEM II/A-V42.5R
Blaine (m^2/kg)	347.0	382.0
Setting times (min)		
Initial	90	90
Final	140	140
Mechanical Strengths at 2 days (MPa)		
Flexion	4.9	5.0
Compression	26.8	26.8

RESULTS AND DISCUSSION

The pastes cured at different temperatures were tested for compressive strength at ages 2, 7, 15 and 28 days. The results are plotted in Figure 1.

According to two of the graphs, compressive strength grew with temperature in the early-age cements (2 days of hydration). These findings concur with prior studies [2, 21], where the early age compressive strength of cement pastes was observed to increase progressively with rising temperature due to accelerated hydration.

For CEM I 42.5R pastes cured at 40°C, compressive strength began to decline after 15 days and then flattened, while in the samples cured at 85°C strength fell sharply after only two days. In blended cement CEM II/A-V42.5R, the compressive strength was higher during the first few days for pastes cured at 40 and 85°C, but subsequently

declined slightly in the pastes cured at 40°C and steeply in the samples cured at 85°C. In specimens cured at 4 and 22°C compressive strength increased steadily across the 28-day period. Compressive strength was observed to develop more slowly in the blended cement, probably because the pozzolanic reactions involved are slow [21]. Overall, the findings clearly showed that the 28-day compressive strength recorded for blended cement CEM II/A-V42.5R was lower at all curing temperatures than the values for ordinary Portland cement CEM I 42.5R. Escalante et al. [19] reported similar results for blended cement containing 30% fly ash during the first year of hydration.

Paste hydration was monitored by X-ray diffraction (XRD). The patterns obtained are given in Figure 2. An analysis of the respective diffractograms showed no substantial differences in mineralogical composition.

Table 3. Total porosity (%).

T(°C)	2 days	28 days
	Cement CEM I 42.5R	
4	17.71	11.98
22	14.47	8.83
40	13.63	7.44
85	14.30	18.95
	Cement CEM II/A-V42.5R	
	16.47	12.45
	16.64	10.70
	13.14	9.30
	12.53	15.45

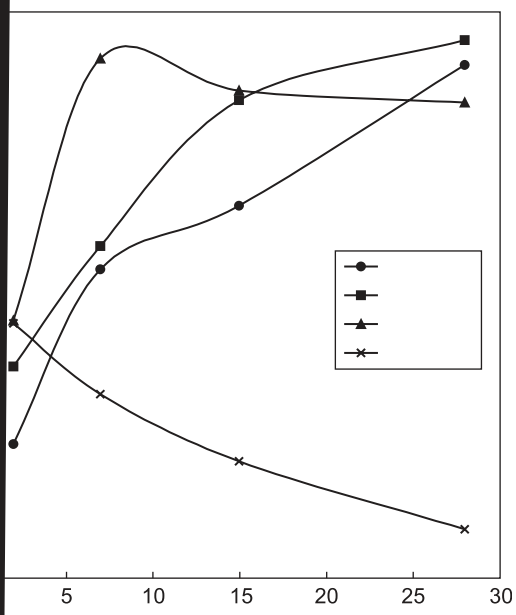

The same crystalline phases were identified in all samples of both cements: anhydrous phases (alite, belite, aluminate and ferrite phases) and hydrated phases (ettringite, and portlandite), and calcite. No silica hydrate C–S–H gel was detected in any of the samples. The XRD findings showed greatest amounts of ettringite, AFt, formed in the pastes cured at 4 and 22°C, while this phase was undetectable at 85°C. According to Skalny et al. [22], ettringite is not stable at temperatures of over 70°C. No monosulphate phases were detected in any of the pastes.

Porosity plays a prominent role in the development of mechanical properties and can provide further information about paste performance. The total porosity data as determined by mercury intrusion porosimetry are consequently given in Table 3. Further to the Table, temperature clearly affected both cements, CEM I 42.5R and CEM II/A-V 42.5R. While total porosity was lower in the two-day pastes when cured at 40 or 85°C than when cured at 4 or 22°C, in the 28-day specimens porosity was higher for the pastes cured at 85°C and lower for the samples cured at 4, 22 and 40°C.

As a general rule, low initial rates of hydration (such as where $4°C \leq T \leq 22°C$) may be said to favour the controlled precipitation of reaction products in interstitial space, raising the gel/space ratio, and with it compressive strength, throughout the curing period. In other words, mechanical strength is closely related to how and where hydration products precipitate as well as to pore size distribution (air, macro- and mesopores). Table 4 gives the pore size distribution findings for 2- and 28-day specimens of both cements.

Table 4. Distribution of pore size in cement pastes (%).

	Size	Temperature (°C)			
		4°C	22°C	40°C	85°C
	CEM I 42.5R				
2 days	Air pores: > 10 μm	2.54	2.28	2.39	3.36
	Macropores: 10-0.05 μm	25.55	13.26	14.99	24.64
	Mesopores: < 0.05 μm	71.90	84.45	82.26	71.99
28 days	Air pores: > 10 μm	3.46	3.59	10.73	1.48
	Macropores: 10-0.05 μm	12.99	7.91	11.86	80.55
	Mesopores: < 0.05 μm	83.53	88.49	77.40	17.96
	CEM II/A-V 42.5R				
2 days	Air pores: > 10 μm	04.07	3.58	2.16	2.79
	Macropores: 10-0.05 μm	20.83	18.47	15.02	26.76
	Mesopores: < 0.05 μm	74.91	77.94	82.82	70.44
28 days	Air pores: > 10 μm	4.41	3.24	15.38	4.01
	Macropores: 10-0.05 μm	15.52	10.11	7.69	28.33
	Mesopores: < 0.05 μm	80.06	86.64	76.92	67.65

Figure 2. XRD patterns of the cement pastes at different curing temperatures.

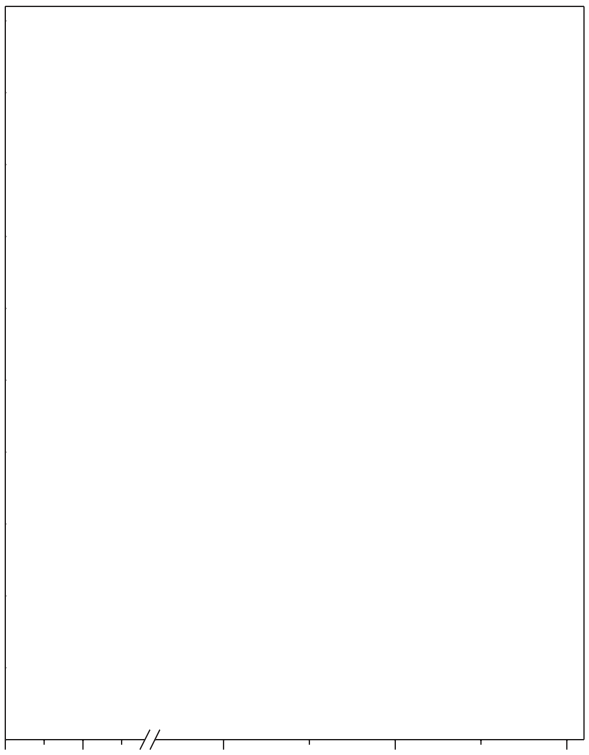

Figure 4. Infrared spectra of cement pastes CEM II/A-V42.5R.

According to these data, in pastes cured at 4 and 22°C, the proportion of macropores decreased and the proportion of mesopores grew with time. The decline in compressive strength after 28 days in pastes hydrated at 40°C was due to an increase in the air pore fraction, while the low 28-day compressive strength in the pastes cured at 85°C was attributed to the high percentage of macropores, since the fraction of mesopores in these specimens was lower than in the pastes hydrated at 22°C, particularly in the case of CEM I 42.5R.

The FTIR spectra for the hydrated pastes are shown in Figures 3 and 4. An analysis of these FTIR spectra confirmed the formation of C–S–H gel in both cements, as denoted by the ν_3 (Si–O) absorption band at 970--978 cm^{-1}. Other bands appearing on the spectra included the stretching vibration at 3460 cm^{-1} characteristic of portlandite O–H bonds and the $\nu_3(SO_4)$ band at 1150 cm^{-1} characteristic of the S–O bond in the SO_4 present in ettringite. The $\nu_3(CO_3)$, $\nu_2(CO_3)$ and $\nu_1(CO_3)$ absorption bands at 1420-1480 cm^{-1}, 840-860 cm^{-1} and 712 cm^{-1}, respectively, confirmed the partial weathering of the paste samples.

A broad absorption band associated with silicates (1000-900 cm^{-1}) appeared on the spectra for the cement pastes cured at 4°C. This band narrowed with rising curing temperatures, however, and was narrowest for the pastes cured at 85°C. This was because a C–S–H gel with a higher order structure formed as curing temperatures increased; moreover, as the degree of paste hydration grew with temperature, the intensity of the vibration bands at around 920 cm^{-1} associated with the anhydrous phases (C_3S and C_2S) declined.

Figures 5 and 6 show CEM I 42.5R and CEM II/ /A-V 42.5R paste morphologies, respectively. While only a few cement grains were hydrated in the two-day CEM I 42.5 R and CEM II/A-V 42.5R samples cured at 4 and 22°C, the pastes cured at 40 and 85°C showed an apparently high degree of hydration, although more reaction product with a less uniform microstructure was observed in the 85°C samples. After 28 days, the matrix in the cement paste hydrated at 4°C was darker and had more C–S–H in the outer zone than the 85°C matrix. At 85°C, by contrast, the hydration products clustered around the unhydrated grains, acting as barriers to

Table 5. Atomic ratio determined by BSE/EDX (CEM I 42.5R).

	Outer				Inner			
	2 days							
	4°C	22°C	40°C	85°C	4°C	22°C	40°C	85°C
Ca/Si	1.90 ± 0.23	2.00 ± 0.23	2.24 ± 0.24	2.30 ± 0.30	2.10 ± 0.33	2.15 ± 0.15	2.17 ± 0.18	2.23 ± 0.25
Al/Si	0.17 ± 0.08	0.16 ± 0.07	0.10 ± 0.03	0.12 ± 0.03	0.05 ± 0.02	0.06 ± 0.02	0.07 ± 0.02	0.07 ± 0.02
Al/Ca	0.07 ± 0.02	0.06 ± 0.02	0.08 ± 0.03	0.07 ± 0.02	0.03 ± 0.01	0.03 ± 0.01	0.03 ± 0.01	0.03 ± 0.01
S/Ca	0.05 ± 0.02	0.06 ± 0.02	0.07 ± 0.01	0.09 ± 0.01	0.03 ± 0.01	0.03 ± 0.01	0.04 ± 0.01	0.06 ± 0.02
	28 days							
	4°C	22°C	40°C	85°C	4°C	22°C	40°C	85°C
Ca/Si	1.74 ± 0.22	1.78 ± 0.13	1.84 ± 0.17	2.39 ± 0.36	2.02 ± 0.34	1.93 ± 0.15	1.98 ± 0.14	2.14 ± 0.27
Al/Si	0.15 ± 0.04	0.16 ± 0.06	0.15 ± 0.06	0.08 ± 0.04	0.07 ± 0.03	0.08 ± 0.03	0.05 ± 0.01	0.06 ± 0.02
Al/Ca	0.07 ± 0.03	0.09 ± 0.03	0.08 ± 0.03	0.05 ± 0.01	0.03 ± 0.01	0.04 ± 0.01	0.03 ± 0.01	0.03 ± 0.01
S/Ca	0.06 ± 0.01	0.07 ± 0.01	0.07 ± 0.02	0.08 ± 0.01	0.03 ± 0.01	0.04 ± 0.01	0.03 ± 0.01	0.07 ± 0.02

Table 6. Atomic ratio determined by BSE/EDX (CEM II /A-V42.5R).

	Outer				Inner			
	2 days							
	4°C	22°C	40°C	85°C	4°C	22°C	40°C	85°C
Ca/Si	1.72 ± 0.13	1.74 ± 0.10	1.80 ± 0.21	1.71 ± 0.10	1.75 ± 0.22	1.90 ± 0.32	1.92 ± 0.11	1.93 ± 0.26
Al/Si	0.17 ± 0.06	0.19 ± 0.06	0.25 ± 0.10	0.23 ± 0.06	0.09 ± 0.02	0.08 ± 0.02	0.10 ± 0.03	0.10 ± 0.02
Al/Ca	0.09 ± 0.02	0.11 ± 0.04	0.13 ± 0.05	0.14 ± 0.05	0.06 ± 0.03	0.04 ± 0.01	0.05 ± 0.02	0.05 ± 0.02
S/Ca	0.05±0.01	0.07±0.02	0.09±0.02	0.09 ± 0.03	0.02 ± 0.01	0.04 ± 0.01	0.04 ± 0.01	0.05 ± 0.02
	28 days							
	4°C	22°C	40°C	85°C	4°C	22°C	40°C	85°C
Ca/Si	1.74 ± 0.12	1.73 ± 0.10	1.68 ± 0.10	1.77 ± 0.15	1.89 ± 0.20	1.92 ± 0.50	1.73 ± 0.16	2.12 ± 0.17
Al/Si	0.17 ± 0.05	0.19 ± 0.07	0.22 ± 0.06	0.16 ± 0.04	0.08 ± 0.02	0.13 ± 0.02	0.10 ± 0.02	0.06 ± 0.02
Al/Ca	0.10 ± 0.03	0.11 ± 0.03	0.13 ± 0.02	0.09 ± 0.03	0.04 ± 0.01	0.05 ± 0.01	0.05 ± 0.02	0.03 ± 0.01
S/Ca	0.05 ± 0.03	0.05 ± 0.03	0.07 ± 0.01	0.08 ± 0.01	0.04 ± 0.01	0.04 ± 0.01	0.05 ± 0.01	0.07 ± 0.01

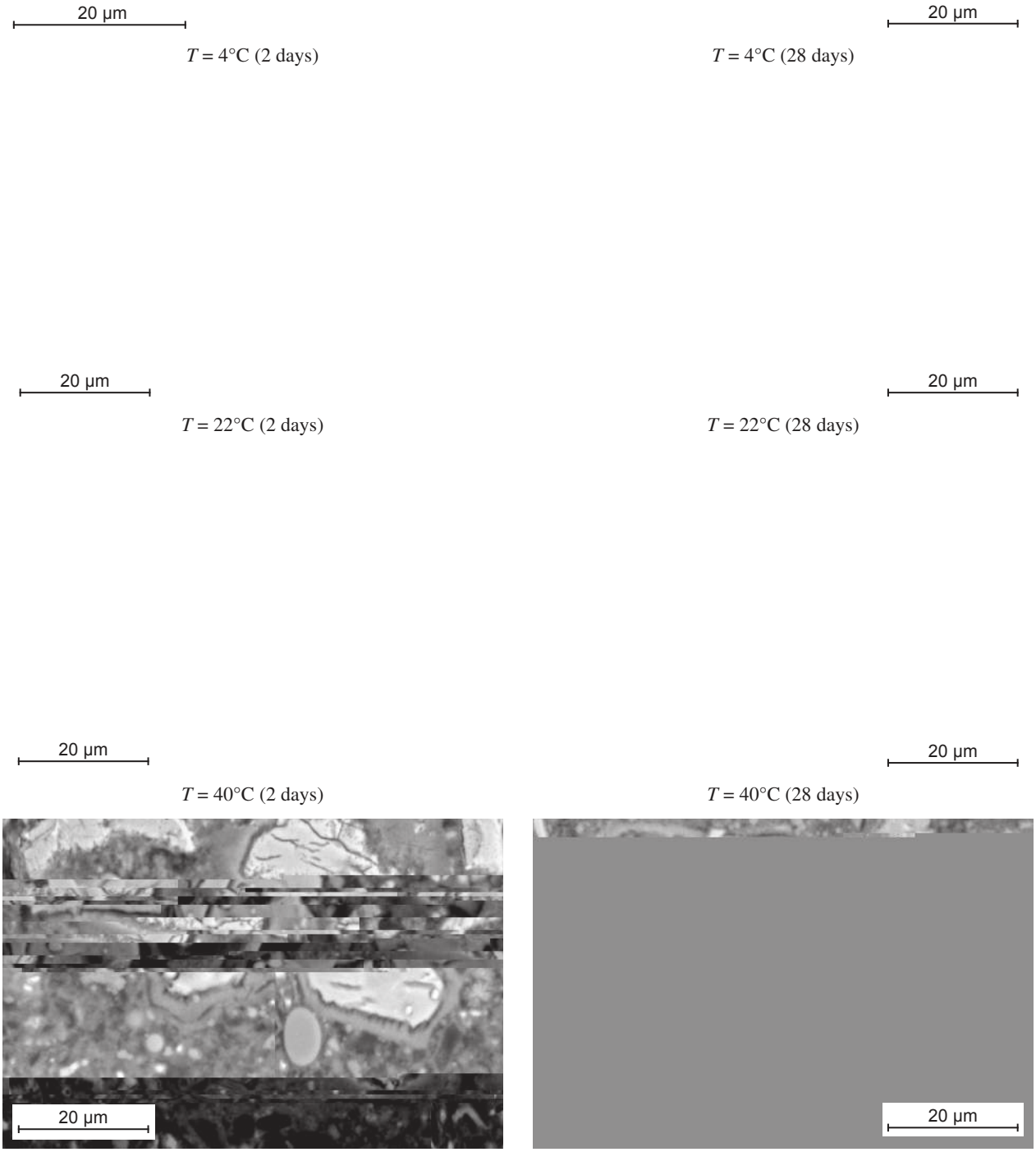

T = 4°C (2 days) *T* = 4°C (28 days)

T = 22°C (2 days) *T* = 22°C (28 days)

T = 40°C (2 days) *T* = 40°C (28 days)

T = 85°C (2 days) *T* = 85°C (28 days)

Figure 5. BSE micrographs of CEM I 42.5R hydrated at different temperatures for 2 and 28 days.

further hydration and retarding the diffusion of the reagents. No ettringite crystals could be identified in these micrographs.

The C–S–H rims forming around the cement grains at 85°C were brighter than the C–S–H gel forming in the pastes cured at lower temperatures. This difference has been reported by other authors [18]. The thickness of the C–S–H rims in 28-day pastes has been estimated to range from 5 μm at 20°C to 25 μm at 85°C.

The micrographs of the 28-day pastes also showed that the samples hydrated at 85°C were more porous, while the 4 and 22°C samples had a more compact structure. Another relevant development was the appearance in the 85°C samples of a thin black rim around the hydrated cement grains, not present in the pastes hydrated at 4, 22 or 40°C. J. I. Escalante at al. [20] interpreted the black rims observed around some cement grains after high temperature hydration to actually be discontinuities within the paste matrix that would have an adverse effect on mechanical properties, while further retarding grain hydration. With compressive strengths that declined substantially, the cement pastes hydrated at 85°C in this study conformed to that interpretation.

Microanalyses were conducted in both the outer (hydration products forming in the space initially containing water) and the inner zones (hydration products forming inside the original cement grains). The atomic ratios estimated by BSE/EDX are listed in Tables 5 and 6.

An analysis of the values showed that in both cements, the samples cured at 85°C had a higher Ca/Si ratio than the pastes cured at lower temperatures. This was very likely due to the abundant initial precipitation of hydration products, which led to the formation of more heterogeneous microstructures and mixes or solid solutions between the C–S–H gel and portlandite [23]. At such a high reaction temperature, this instrumental technique was unable to yield accurate values for the Ca/Si ratios in the gel.

In the fly ash-containing blended cement, CEM II/A-V42.5R, pozzolanic activity entailed the uptake of Ca^{2+} ions needed to form additional C–S–H gel. Such

Figure 7. ^{29}Si MNR of cement pastes hydrated during 28 days.

pozzolanic activity induces differences, essentially in the inner C–S–H product. In the blended cement pastes, for a given temperature, the Ca/Si ratio in the inner C–S–H may be lower than the ratio in plain cement, for the Al/Ca ratio increases with the uptake of replacement material and the S/Ca ratio rises with temperature in both cements.

^{29}Si nuclear magnetic resonance (MAS NMR) was used to monitor cement hydration taking place at 4 and 85°C. The spectra in Figure 7 represent the ^{29}Si MAS NMR findings, respectively, for CEM I 42.5R and CEM II/A-V42.5R pastes hydrated at the experimental temperatures for 28 days.

The ^{29}Si MAS NMR spectra exhibited four types of resonance peaks: Q^0 (from -69 to -74 ppm) attributed to the SiO_4 tetrahedral monomer in the alite and belite phases; and three further peaks, at -79 ppm, -82 ppm and -85 ppm assigned to Q^1, Q^2 (1Al) and Q^2 (0Al) Si units, respectively due to C–S–H gels formed in the hydration process. The relative proportions of silicon associated with the Q^0, Q^1 and Q^2 configurations were determined by deconvoluting the spectra and measuring the area associated with each peak (Table 7). The results obtained were consistent with the acceleration of hydration reactions at rising temperatures and the conversion of the anhydrous Q^0 species to Q^1 and Q^2 units.

The intensity of Q^2 (0Al) increased significantly with temperature and exceeded the number of Q^1 units in the CEM II/A-V42.5R pastes after 28 days, increasing $\sum Q^2/Q^1$. In addition, the average chain length (*LMC*) was calculated from the deconvolution data found for the ^{29}Si NMR spectra into the following equation [24]:

$$LMC = [Q^1 + Q^2 + 3/2Q^2(1Al)]/0.5Q^1$$

The results obtained (Table 7) showed that in both cements the average chain length and degree of hydration increased with temperature.

CONCLUSIONS

The main conclusions to be drawn from the present study are as follows:

In both cements (with and without fly ash), increasing the curing temperature accelerated the early age hydration reactions, as reflected in the initial increase in mechanical strength. After 28 days, however, strength declined steeply in the pastes cured at 85°C, while it rose gradually with time in the pastes cured at 22 and 40°C.

As a general rule, low initial rates of hydration (such as with $4°C \leq T \leq 22°C$) may be said to favour the controlled precipitation of reaction products in interstitial space, raising the gel/space ratio, and with it, compressive strength throughout the curing period. In other words, mechanical strength is closely related to how and where hydration products precipitate, as well as to pore size distribution (air, macro- and mesopores).

Table 7. Deconvolution data of ^{29}Si NMR spectra of cement pastes CEM I 42.5R and CEM II/A-V42.5R (28 days).

T (°C)	Q^0 (C_3S, C_2S)	Q^1 (0Al)	Q^2 (1Al)	Q^2 (0Al)	$\sum Q^2/Q^1$	LMC	Degree of hydration
			CEM I 42.5R				
4°C	-69.90 ppm -71.69 ppm -73.79 ppm -75.80 ppm *I* = 60.24%	-79.3 ppm *I* = 23.24%	-82.47 ppm *I* = 9.78%	-84.7 ppm *I* = 6.74%	0.71	3.84	39.76%
85°C	-69.9 ppm -71.64 ppm -73.75 ppm -75.87 ppm *I* = 48.90%	-79.20 ppm *I* = 17.66%	-82.00 ppm *I* = 15.56%	-85.25 ppm *I* = 17.87%	1.89	6.67	51.10%
			CEM II/A-V 42.5R				
4°C	-69.95 ppm -71.64 ppm -73.30 ppm -74.80 ppm *I* = 56.90%	-78.60 ppm *I* = 20.95%	-82.00 ppm *I* = 14.62%	-85.0 ppm *I* = 7.53%	1.06	4.81	43.10%
85°C	-69.60 ppm -71.60 ppm -73.60 ppm -75.65 ppm *I* = 47.02%	-79.00 ppm *I* = 18.89%	-82.00 ppm *I* = 13.24%	-85.12 ppm *I* = 20.83%	1.82	6.31	52.98%

Curing temperature was found to affect the composition of the C–S–H gels formed in the cement paste: the average chain length was longer in the gels formed at high than at low temperatures.

No substantial temperature-induced differences were found between cements with and without fly ash additions.

References

1. Ortiz Lozano J. A., Aguado de Cea A., Agulló L., García Vicente T., Zermeño de León M. E.: Materiales de Construccion. *58*, 291 (2008).
2. Elkhadiri I., Puertas F.: Construction and Building Materials *22*, 1331 (2008).
3. Verbeck J. G., Helmuh R. H.: Proc. 5th Int. Cong. Chem. Cem., Vol. 3, pp. 1-32 Tokyo, Japan 1968.
4. Olivares M., Laffarga J., Galán C., Nadal P.: Materiales de Construcción *53*, 273 (2003).
5. Kjellsen K. O., Detwiller R. J., Gjov O. D.: Cement and Concrete Research *21*, 179 (1991).
6. Kjellsen K. O., Detwiller R. J., Gjov O. D.: Cement and Concrete Research *20*, 308 (1990).
7. Cao Y., Detwiler R. J.: Cement and Concrete Research *25*, 627 (1995).
8. Patel H. H., Bland C. H., Poole A. B.: Cement and Concrete Research *25*, 485 (1995).
9. Al-Dulaijan S. U., Parry-Jones G., Al Tayyib A. H. J., Al-Mana A. I.: Journal of American Ceramic Society *73*, 736 (1990).
10. Parry-Jones G., Al-Tayyib A. H. J., Al-Mana A. I.: Cement and Concrete Research *18*, 229 (1988).
11. Parry-Jones G., Al-Tayyib A. H. J., Al-Dulaijin S. U., Al-Mana, A. I.: Cement and Concrete Research. *19*, 228 (1989).
12. Bentur A., Berger R. L., Kung H. J., Milestone N. H., Young J. F.: Journal of American Ceramic Society *62*, 362 (1979).
13. Hirljac J., Wu Z. Q., Young J. F.: Cement and Concrete Research *13*, 77 (1983).
14. Regourd M., Gautier E. : Béton *387*, 83 (1980).
15. Kjellsen K. O. : Cement and. Concrete Research *26*, 295 (1996).
16. Scrivener K. L.: Cement and Concrete Research *22*, 1224 (1992).
17. Scrivener K. L., Taylor H. F. W.: Advances in Cement Research *5*, 20, 139 (1993).
18. Famy C., Scrivener K. L., Atkinson A., Brough A. R.: Cement and Concrete Research *32*, 269 (2002).
19. Escalante-García J.I., Sharp J.H.: Cement and Concrete Research 31, 695 (2001).
20. Escalante-García J. I., Sharp J. H.: Cement and Concrete Research *28*, 1259 (1998).
21. Halse Y., Jensen H. U., Pratt P. L.: Proc. 8th Int. Cong. Chem. Cem., Vol. IV, p.176, Rio de Janeiro 1986.
22. Skalny J., Johansen V., Thaulow N., Palomo A: Materiales de Construcción *46*, 244 (1996).
23. Taylor H. F. W.: Advances in Cement Based Materials *1*, 38 (1993).
24. Richardson I. G.: Cement and Concrete Research *29*, 1131 (1999).